A DUAL-WAVELENGTH QUANTUM CASCADE LASER WITH TWO OPTICAL TRANSITIONS IN EACH ACTIVE REGION

K.J. Franz, K.T. Shiu, S.R. Forrest,* and C. Gmachl

Department of Electrical Engineering and
Princeton Institute for the Science and Technology of Materials (PRISM),
Princeton University, Princeton, NJ 08544, USA
** Department of Electrical Engineering and Computer Science and*
Department of Physics,
University of Michigan, Ann Arbor, MI 48109, USA
Email address: kfranz@princeton.edu

Abstract

We report on a novel quantum cascade laser design that utilizes wide active region quantum wells to create a lasing transition between the second- and first-excited states of the constituent wells. Electroluminescence and lasing spectra confirm the presence of the optical transition at the expected energy, but also show the conventional transition between energy levels resulting from excited and ground states of the original quantum wells. As a result, the laser produces simultaneous dual-wavelength emission at 8.2 μm and 9.3 μm.

I. Introduction

Quantum Cascade (QC) lasers have made possible the development of mid-infrared technologies—such as room temperature and compact trace gas sensing systems—that, before the QC laser's invention in 1994 [1,2], were not feasible due to the lack of a high performing mid-infrared laser. Performance progress of QC lasers has historically been made on two fronts: improved quantum design [3,4] and improved growth and processing techniques [5]. The accelerating flow of literature reporting advances in QC lasers strongly suggests optimality has yet to be reached. For example, QC laser functionality is advancing through higher-performing designs (e.g. for low threshold, high temperature, and continuous wave operation) [3] and through novel unconventional active region design concepts [4].

Here we report on a two quantum well QC laser that utilizes the second- and first-excited states of the constituent quantum wells of the active region—in contrast to the first-excited and ground states, as in conventional QC lasers. This excited state architecture has the potential for improving QC laser performance in two ways. First, the dipole matrix element between consecutive higher-level states is in general larger than between lower-level states. Second, wider active region wells reduce the effects of scattering caused by interface roughness.

The gain coefficient g of a QC optical transition between an upper u and lower l state is given by

$$g = \tau_u \left(1 - \frac{\tau_l}{\tau_{ul}}\right) \frac{4\pi e}{\varepsilon_0 n_{eff} \lambda_0 L_p} \frac{z_{ul}^2}{\Gamma_{ul}} \tag{1}$$

where τ_u is the non-radiative scattering time of the upper state, τ_l the non-radiative scattering time of the lower state, and τ_{ul} the scattering time between the upper and lower state; e is the electron charge, n_{eff} the effective refractive index of the laser mode, λ_0 the free space wavelength, and L_p the length unit of gain of one period of active and injector region the QC structure; z_{ul} is the optical dipole matrix element, and Γ_{ul} the full-width at half-maximum (FWHM) of the transition as measured from the luminescence spectrum [2].

As can be seen from Eq. (1), gain increases with the square of the optical dipole matrix element z_{ul}. Therefore, steps that increase this value enhance the laser performance. Fig. 1 illustrates how the optical dipole matrix element evolves for the intersubband transitions between adjacent states for a single InGaAs/AlInAs:InP quantum well. Here, the optical dipole matrix element of a specific transition is calculated after adjusting the quantum well width to give a transition energy ε_{ul} of 125 meV. As can be seen, the optical dipole matrix element increases for higher lying transitions. Thus an optical transition between the second- and first-excited states of a quantum well will have a greater gain coefficient than a first-excited to ground state transition of equal energy. In the context of this specific QC laser description, we refer to a "ground state" as any state that originated from the true ground state of a constituent quantum well and accordingly for the excited states.

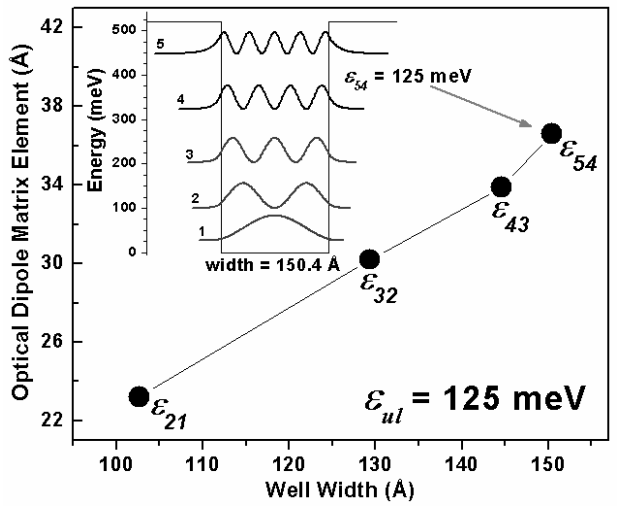

Fig. 1: The calculated optical dipole matrix element of the specified transition, where well width has been adjusted to give a transition energy ε_{ul} = 125 meV. For the constant transition energy ε_{ul} = 125 meV, the optical dipole matrix element and quantum well width increase for transitions between higher lying levels. Here we simulate optical transitions in the InGaAs/AlInAs:InP system, which has a conduction band offset of 520 meV. The inset illustrates a quantum well with an energy difference of 125 meV between states 5 and 4. The moduli squared of states 1 through 5 are shown with the baseline corresponding to the energy of each state.

One should note that a tradeoff exists between the increase in the optical dipole matrix element from using higher excited states and the accompanying decrease in the magnitude of the population inversion—which is proportional to $\tau_u(1-\tau_l/\tau_{ul})$ in Eq. (1)—due to a decrease in upper state lifetime τ_u. This upper state lifetime is decreased for the excited-state laser because of the larger number of lower empty levels into which electrons can scatter. Still, calculations confirm the effect of a larger optical dipole dominates the effect of the decreased population inversion.

The second advantage of using an excited state optical transition comes from the necessity of using wider wells, as shown in Fig. 1. Interface roughness at transitions between well and barrier material creates modifications of wavefunctions with respect to the ideal case of zero roughness at the interfaces. This surface roughness ultimately results in broadening of the emission spectrum Γ_{ul}, which reduces the gain coefficient g, as shown in Eq. (1). Interface roughness is a property of the growth quality and is usually on the order of one to two monolayers. Separate from improving the quality of the growth, the effects of interface roughness are reduced in wider wells, which intuitively can be motivated by the fact that the region of roughness is relatively smaller in wider wells. Theoretical and experimental results of broadening due to interface roughness have been discussed in Ref. [6].

Due to the finite conduction band offset used for our quantum wells, this excited-state concept is especially suited for longer wavelength lasers where the second-excited state is more easily confined.

II. Laser design and fabrication

The laser was grown with a Riber 32 gas-source MBE on a low-doped ($n < 2x10^{17}$ cm^{-3}) InP:S substrate. The active and injector region layer sequence of one period is (in angstroms, starting from the injection barrier ***I*** going right to left in Fig. 1) **40**/100/**16**/88/**16**/36/**12**/36/**12**/20/**20**/28/**20**/20/**24**/16/**28**/24, where $In_{0.52}Al_{0.48}As$ barrier layers are in bold, $In_{0.53}Ga_{0.47}As$ well layers are in normal text, and Si-doped 2×10^{17}cm^{-3} layers are underlined. Fig. 2 shows the electron energy band diagram. Forty active region-injector periods were used for the active core, and were clad on top and bottom by 0.55 μm InGaAs ($n = 5\times10^{16}$ cm^{-3}). A 0.9 μm InP ($n = 5\times10^{16}$ cm^{-3}) buffer layer was grown before the bottom InGaAs cladding. After the top InGaAs cladding, an additional 4.2 μm InP ($n = 5\times10^{16}$ cm^{-3}) and 1.2 μm InP ($n = 6.7\times10^{18}$ cm^{-3}) were grown, before capping the growth with 0.06 μm InGaAs ($n = 2\times10^{19}$ cm^{-3}). The lasers were processed as deep-etched ridge waveguide lasers with stripe widths ranging from 9 to 15 μm by conventional photolithography and wet chemical etching, and were electrically insulated by 0.3 μm thick PECVD-deposited SiN_x. After evaporation of the Ti/Au (30nm/300nm) top contact, the sample was thinned to ~200 μm and the back Ge/Au (30nm/300nm) contact was evaporated. The laser bars were cleaved to 2.5 mm cavity length, mounted epilayer up on a Cu heat sink with In solder, and wire bonded.

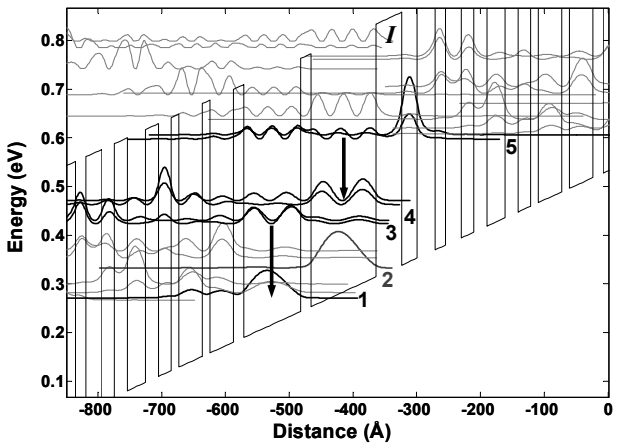

Fig. 2: Conduction band diagram of an active region embedded between two injector regions with the moduli squared of the relevant wavefunctions of a two transition QC laser. An electric field of 60 kV/cm is applied. Arrows indicate optical transitions at 8.1 μm and 9.8 μm. The numbering of the energy levels here is unrelated to the numbering in Fig. 1.

At the design field of 60 kV/cm, the excited state laser transition (levels 5 → 4) has a simulated energy of 127 meV (λ = 9.76 μm) with an optical dipole matrix element z_{54} = 3.42 nm. We observe this laser emission at λ ~ 9.3 μm, in good agreement with calculations, given a few percent uncertainty in the thickness of barriers and wells. Energy levels 4 and 3 are separated by an energy of about one optical phonon for rapid emptying of level 4 and population inversion of the energy transition 5 → 4.. Experimentally, we further observe laser action at λ ~ 8.2 μm, which we attribute to a transition between levels 3 and 1 of the active core. This lower laser transition has a designed energy of 153 meV (λ = 8.09 μm) and an optical dipole matrix element of z_{31} = 1.28 nm at the design field. The waveguide loss is estimated at 7.5 cm^{-1} for λ = 9.76 μm and 5.0 cm^{-1} for λ = 8.09 μm; the confinement factor for the active core is 60.2% and 66.6% for the two wavelengths, respectively.

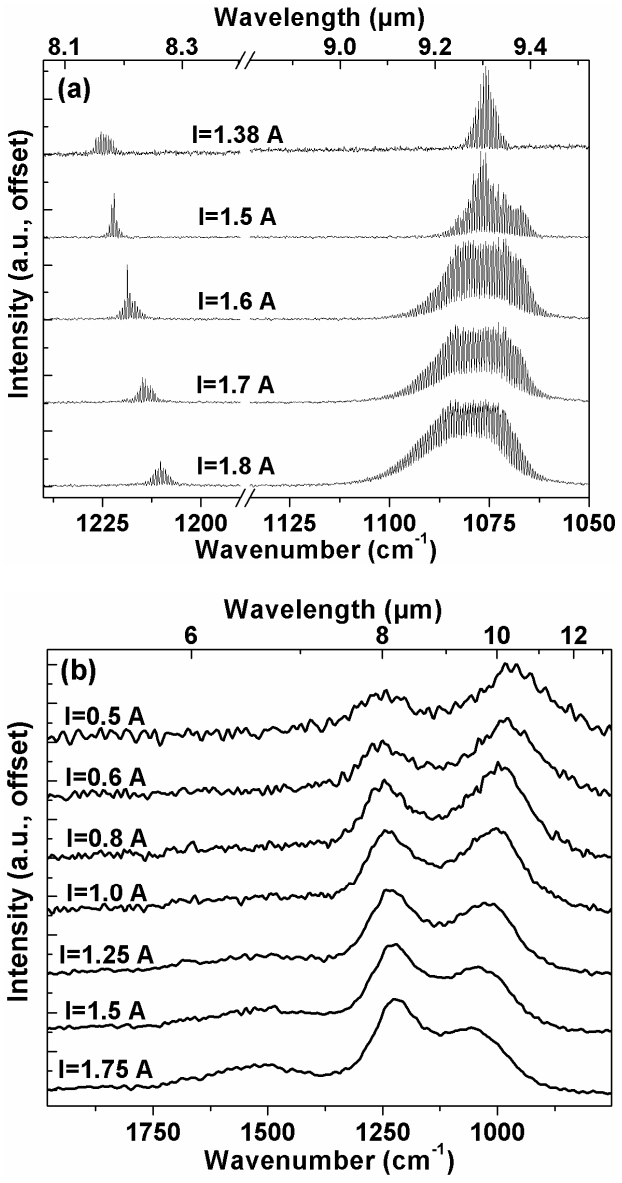

Fig. 3: (a) Fabry-Perot laser spectra obtained from a 9.0 μm x 2.5 mm QC laser at 80 K for various pulsed peak currents, as indicated. (b) Electroluminescence spectra of a 0.027 mm^2 partially circular mesa measured at 80 K for various current levels.

III. Analysis of laser characteristics and performance

Fig. 3(a) shows the 80 K pulsed mode Fabry-Perot spectral characteristics of a 9.0 μm x 2.5 mm laser. Lasing occurs nearly simultaneously at 8.2 μm (151 meV) and 9.3 μm (133 meV). Laser emission at 9.3 μm is generally more powerful than at 8.2 μm. The apparent simultaneous turn-on of the lasers is not consistent with calculated thresholds of 0.33 kA/cm^2 for the 9.3 μm transition and 1.56 kA/cm^2 for the 8.2 μm transition, which raises interesting questions with regards to the extent to which the two lasers are coupled.

As the applied electric field increases, the shorter-wavelength peak red-shifts while the longer-wavelength peak blue-shifts. Fig. 3(b) shows electroluminescence spectra of deep-etched partially-circular mesas, allowing the observation of optical transition energies in the absence of gain narrowing. Again, two distinct energy peaks are measured, with the distance between the two decreasing with increasing field. In the range of our power source, the peak of the lower energy transition tunes between 9.48 and 10.50 μm (131-118 meV), and the peak of the higher energy transition tunes from 8.21 to 7.95 μm (151-156 meV). These two peaks are in good agreement with the optical transitions 5 → 4 and 3 → 1 in Fig. 2. At higher fields, a third peak is seen in the electroluminescence shown in Fig. 2(b) around 6.46 μm (192 meV). We identify this peak as the 4 → 1 transition, calculated to be at 6.42 μm (193 meV). Fig. 4 shows the

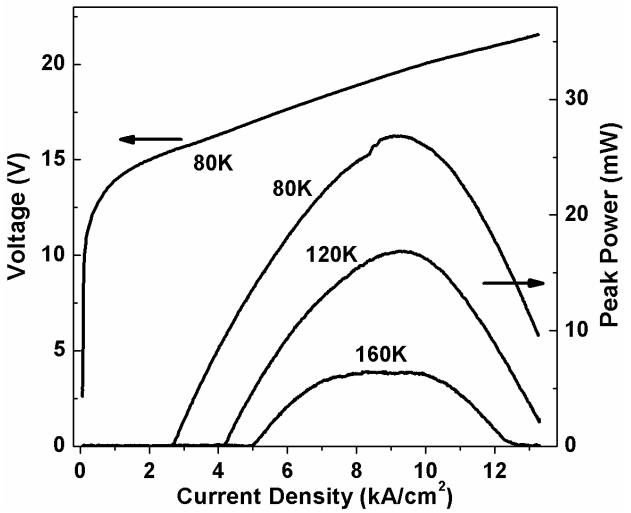

Fig. 4: Light output and voltage vs. current characteristics of a 12.5 μm x 2.5 mm QC laser at various heat sink temperatures.

pulsed light and voltage versus current characteristics for a 12.5 μm x 2.5 mm laser ridge. Threshold current densities for the first lasers of this kind were measured as 2.63 kA/cm^2 at cryogenic temperatures.

IV. Conclusion

We designed and fabricated a laser that uses the second- and first-excited states of the constituent active region quantum wells as the primary laser transition. We observed simultaneous lasing at wavelengths of 8.2 μm and 9.3 μm resulting from two consecutive optical transitions within each active region.

Acknowledgements

K.J.F. gratefully acknowledges the financial support of the National Science Foundation Graduate Research Fellowship Program. This work was partially supported by DARPA-LPAS.

References

[1] J. Faist, F. Capasso, D.L. Sivco, C. Sirtori, A. L. Hutchinson and A.Y. Cho, "Quantum cascade laser," *Science* **264**, 553-556 (1994)

[2] C. Gmachl, F. Capasso, D.L. Sivco and A.Y. Cho, "Recent progress in quantum cascade lasers and applications," *Rep. Prog. Phys.* **64,** 1533–1601 (2001).

[3] D. Hofstetter, M. Beck, T. Aellen, and J. Faist, "High-temperature operation of distributed feedback quantum-cascade lasers at 5.3 μm," *Appl. Phys. Lett.* **78**, 396-398 (2001).

[4] C. Sirtori, A. Tredicucci, F. Capasso, J. Faist, D.L. Sivco, A.L. Hutchinson, and A.Y. Cho, "Dual-wavelength emission from optically cascaded intersubband transitions," *Opt. Lett.* **23**, 463-465 (1998); A. Tredicucci, C. Gmachl, F. Capasso, D.L. Sivco, A.L. Hutchinson, and A.Y. Cho, "A multiwavelength semiconductor laser," *Nature* **396**, 350-353 (1998).

[5] M. Beck, D. Hofstetter, T. Aellen, J. Faist, U. Oesterle, M. Ilegems, E. Gini, and H. Melchior, "Continuous wave operation of a mid-infrared semiconductor laser at room temperature," *Science* **295**, 301-305 (2002); A. Matlis, S. Slivken, A. Tahraoui, K.J. Luo, J. Diaz, Z. Wu, A. Rybaltowski, C. Jelen,, and M. Razeghi, "Low-threshold and high power λ~9.0 μm quantum cascade lasers operating at room temperature," *Appl. Phys. Lett.* **77**, 1741-1743 (2000); M. Troccoli, S. Corzine, D. Bour, J. Zhu, O. Assayag, L. Diehl, B.G. Lee, G. Hofler and F. Capasso, "Room temperature continuous-wave operation of quantum-cascade lasers grown by metal organic vapour phase epitaxy," *Electron. Lett.* **41**, 1059-1060 (2005).

[6] S. Tsujino, A. Boark, E. Müller, M. Scheinert, C.V. Falub, H. Sigg, D. Grützmacher, M. Giovannini, and J. Faist, "Interface-roughness-induced broadening of intersubband electroluminescence in p-SiGe and n-GaInAs/AlInAs quantum-cascade structure," *Appl Phys. Lett.* **86**, 062113 (2005).